

High pressure Raman study of $\text{La}_{1-x}\text{Ca}_x\text{MnO}_{3-\delta}$ manganites

A. Sacchetti¹, T. Corridoni², E. Arcangeletti³, P. Postorino³

¹*Laboratorium für Festkörperphysik, ETH-Zürich, CH-8093 Zürich, Switzerland*

²*Dipartimento di Fisica Università di "Roma Tre",
Via della Vasca Navale 84, I-00146 Roma, Italy*

³*"Coherentia" CNR-INFM and Dipartimento di Fisica,
Università di Roma "La Sapienza", Piazzale Aldo Moro 2, I-00185 Roma, Italy*

(Dated: November 30, 2018)

We report on a high-pressure Raman study on two members of the $\text{La}_{1-x}\text{Ca}_x\text{MnO}_{3-\delta}$ manganite family ($x = 0.20$, $\delta = 0$ and $\delta = 0.08$). The results obtained for the $\delta = 0$ sample show a different behavior in the low and high pressure regimes ascribed to the onset of a new pressure-activated interaction previously invoked in other manganite compounds. The comparison of our results with literature data gives further support to the identification of the Jahn-Teller active stretching mode and shows that pressure-induced octahedral symmetrization is more effective in systems exhibiting a lower metallic character. On the contrary the new interaction sets in at pressure which decreases on increasing the metallic character of the system indicating a relevant role of the Mn-Mn hopping integral in its activation.

PACS numbers:

The peculiar properties of colossal magneto-resistive (CMR) mixed-valence manganites^{1,2} are commonly described in the framework of double exchange mechanism³ which competes with the localizing electron-phonon coupling (EPC) triggered by the Jahn-Teller (JT) distortion of the Mn^{+3}O_6 octahedra.⁴ Nevertheless, the effects of the delicate balance among these interactions on the macroscopic properties of these systems are not yet completely understood.² Moreover, in recent years a number of experiments carried out on manganites under pressure pointed out the relevance of a pressure-activated localizing interaction which leads the system towards a new unpredicted high pressure regime.^{5,6,7,8,9,10,11,12,13,14}

Usually, pressure-induced lattice compression in CMR manganites remarkably affects the insulator to metal transition temperature, T_{IM} , since the charge delocalization extent is directly related to both the EPC strength and the hopping integral. In principle, applying pressure results in an Mn-O-Mn bond length compression and consequent linearization (i.e. an increase of the hopping integral) and in a symmetrization the JT distorted MnO_6 octahedra (i.e. a reduction of the EPC). According to the above prediction, early pressure-experiments showed an almost linear increase of T_{IM} within the 0 – 2 GPa pressure range,^{15,16,17,18,19,20,21} whereas recent experiments carried out over much wider pressure ranges showed that the observed low-pressure (LP) behavior cannot be extended to the high-pressure (HP) regime. Indeed, pressure becomes progressively less effective in increasing T_{IM} and a saturation regime where T_{IM} is no more dependent on pressure, is achieved^{6,7}. In several cases, when the saturation regime sets in rather early (around 4-5 GPa), further increase of pressure causes the opposite dependence with T_{IM} starting to decrease^{9,10,11,12,13}.

Among the different investigated manganite compounds, a rather complete set of high pressure (0~15 GPa) experimental data (Raman,⁵ Infrared,⁷ resistivity, x-ray,⁶ and neutron²² diffraction) is available

only for $\text{La}_{0.75}\text{Ca}_{0.25}\text{MnO}_3$ (LC25S). In particular, a HP Raman study of LC25S has shown a remarkable and almost linear hardening of the peak frequency of the JT-active stretching mode on increasing pressure up to 7 GPa, as expected when the JT distortion is reduced. On the contrary, the peak frequency remains almost constant on further increasing the pressure up to 15 GPa.⁵ A good agreement is found with X-ray diffraction data which show a pressure-induced reduction of the JT distortion over the LP regime.⁶ A two-regime behavior for LC25S was also observed in temperature and pressure dependent mid-infrared measurements aimed at determining the insulator-to-metal transition curve. Indeed, T_{IM} increases from 220 K to ~300 K going from zero to ~7 GPa but it keeps almost constant on further increasing the pressure. Additional far-infrared measurements pointed out at the failure of pressure in completely filling the insulating gap at room temperature and in leading the system towards a coherent transport regime.⁸ The whole of the data indicates the onset of the new localizing mechanism which, at room temperature, competes with the *natural* charge-delocalizing tendency of pressure and prevents both the full quenching of the JT distortion and the metallization transition. Finally, the comparison between the above experimental results and the theoretical calculations presented in Ref. 14 suggests the activation of an antiferromagnetic super-exchange coupling, which is in conflict with the *natural* pressure induced charge delocalization, to be responsible for the anomalous high-pressure behavior of LC25S.

In the present paper we focus on the effect of hole doping on the high-pressure behavior of CMR La-Ca manganites to gain a deeper understanding of the pressure effects and to find precursor phenomena of the localizing mechanism. Hole doping, which converts Mn^{+3} into Mn^{+4} , can be varied by changing either Ca-concentration x or oxygen stoichiometry in $\text{La}_{1-x}\text{Ca}_x\text{MnO}_{3-\delta}$ compounds. Indeed, since oxygen is an electron acceptor,

oxygen deficiencies reduce the number of holes, which leads to an effective hole-doping $x_{eff} = x - 2\delta$. Owing to the different ionic radii of La^{3+} and Ca^{2+} (see Ref. 23), Ca-doping induces a moderate reduction of the unit cell volume, whereas oxygen-deficiency induces negligible structural modifications.²⁴ Exploiting oxygen non-stoichiometry it is possible to change the hole doping with negligible structural effects, differently from what happens with Ca-substitution.

We report on high-pressure Raman measurements on two samples of $\text{La}_{0.80}\text{Ca}_{0.20}\text{MnO}_{3-\delta}$ with $\delta = 0.00$ and 0.08 , which corresponds to $x_{eff} = 0.20$ and 0.04 respectively. We remark that such a large hole-density variation is accompanied by a small change in the unit cell volume (0.8% according to Ref. 25). The stoichiometric sample has the same ground-state properties as LC25S, i.e. it is a ferromagnetic metal below Curie temperature $T_C = 194$ K, while the oxygen reduced sample is an insulator at all temperatures, with a ferromagnetic insulating phase below $T_C = 163$ K. Preparation and characterization of powder $\text{La}_{0.80}\text{Ca}_{0.20}\text{MnO}_3$ (LC20S) and $\text{La}_{0.80}\text{Ca}_{0.20}\text{MnO}_{2.92}$ (LC20D) were described in Ref. 25. High pressure far infrared measurements on these sample were also reported in Ref. 8.

Room temperature Raman spectra were collected using a confocal-microscope Raman spectrometer with the same experimental setup and conditions as described in Ref. 5. We just recall that the low frequency cutoff of the notch filter prevents the collection of reliable spectra below 200 cm^{-1} . Samples was pressurized using a diamond anvil cell (DAC). The same sample loading procedure as in Ref. 5 was followed, where fine sample grains were placed on an NaCl pellet pre-sintered in the DAC. This loading procedure ensures rather good hydrostatic conditions and prevents laser-induced sample heating⁵. At each pressure, four Raman spectra were collected from different points of the sample, in order to average over possible preferred orientations of the grains impinged by the laser spot, $\sim 10 \mu\text{m}^2$ on the sample surface in this configuration.

Representative Raman spectra of LC20S and LC20D collected at different pressure are shown in Fig. 1 (a) and (b) respectively. All the spectra show four rather well defined phonon peaks: $\nu_1 \sim 250 \text{ cm}^{-1}$, $\nu_2 \sim 330 \text{ cm}^{-1}$, $\nu_3 \sim 490 \text{ cm}^{-1}$, and $\nu_4 \sim 620 \text{ cm}^{-1}$ at the lowest pressure. These peaks can be assigned to the octahedron modes $A_g(2)$ (b -axis rotation), $B_{3g}(4)$ (c -axis rotation), $A_g(3)$ (apical oxygen bending), and $B_{2g}(1)$ (in-plane oxygen stretching), respectively.^{5,26} Although this assignment is still debated,²⁷ in the following we refer to the two peaks at the highest frequencies (ν_3, ν_4) as bending (ν_B) and stretching (ν_S) phonons, since further support to this assignment is here provided. Raman spectra were

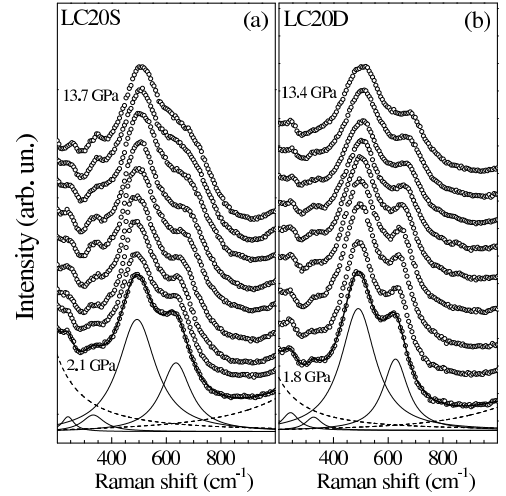


Figure 1: Raman spectra of LC20S (a) and LC20D (b) at selected pressures (open symbols). Data were progressively up-shifted for clarity. Best-fit curves (thick solid line) and fitting components (solid lines: phonons, dashed lines: electronic and high frequency diamond contributions) are also shown for both samples at the lowest pressure.

fitted using the model curve⁵:

$$S(\nu) = [1 + n(\nu)] \left[\frac{A\nu\Gamma}{\nu^2 + \Gamma^2} + \sum_{i=1}^5 \frac{A_i\nu\Gamma_i}{(\nu^2 - \nu_i^2)^2 + \nu^2\Gamma_i^2} \right] \quad (1)$$

where $n(\nu)$ is the Bose thermal population factor, while the first term in square brackets accounts for low-frequency diffusive scattering from carriers with typical lifetime Γ^{-1} . The linear combination of damped harmonic oscillators accounts for the phonon contributions and for the broad structure at around 1100 cm^{-1} , due to the diamond fluorescence background. Good fitting results were obtained for all the spectra using the model of eq. 1 (see Fig. 1). At each pressure, the best-fit parameter values resulting from the analysis of the spectra collected from the four zones were averaged and the maximum dispersion value was taken as the data uncertainty. The rather small dispersion found for the best-fit values of the phonon frequency ν_i and linewidth Γ_i shows that no large pressure gradients are present. Owing to the low-frequency cutoff, the relevant parameters for the electronic contribution are affected by rather large uncertainties and do not show any defined pressure dependence. The frequency and the linewidth of the two low-frequency phonons (ν_1, ν_2 and Γ_1, Γ_2) remain constant within the uncertainty over the whole pressure range, whereas the same quantities for bending and stretching phonons (ν_B, ν_S and Γ_B, Γ_S) exhibit a remarkable pressure dependence. The pressure dependencies of ν_S and ν_B are shown in Fig. 2 (a) and (b) for LC20S and LC20D, respectively, in comparison with the corresponding data on LC25S from Ref. 5.

A pressure induced hardening of ν_B and ν_S frequencies is observed in all the three samples (see Fig. 2), with a pressure rate much higher for ν_S than for ν_B . Moreover, in LC20S and LC25S a two-regime behavior is well evident in the ν_S pressure dependence (i.e. linear and almost pressure independent at low and high pressure, respectively).

Within the LP regime, experimental $d\nu_S/dP$ and $d\nu_B/dP$ were obtained for LC20S, LC20D and compared with literature data for LC25S⁵ and for the parent compound LaMnO₃²⁸. It is worth to notice that the pressure derivatives in LaMnO₃ were obtained considering the Raman spectra up to about 8 GPa only, because the onset of a phase separation regime splits the stretching peak into two components at higher pressures²⁸. The pressure derivatives are shown in the insets of Fig. 2: $d\nu_S/dP$ vs. effective doping x_{eff} and $d\nu_B/dP$ vs. Ca concentration x . We remark that plotting the data vs x or x_{eff} shows a difference only for the non-stoichiometric sample LC20D ($x \neq x_{eff}$). Undoped LaMnO₃ ($x = x_{eff} = 0$) shows nearly the same rate for ν_S and ν_B whereas, on increasing the doping, $d\nu_S/dP$ increases and $d\nu_B/dP$ decreases. Moreover, focusing on the comparison between LC20S ($x = x_{eff} = 0.20$) and LC20D ($x = 0.20, x_{eff} = 0.04$), it appears that $d\nu_B/dP$ depends on x and not on x_{eff} , since both the samples show the same rate $d\nu_B/dP$, whereas $d\nu_S/dP$ exhibits a linear dependence only when the data are plotted as a function of x_{eff} .

Bearing in mind that the number of Mn⁺³ centered octahedra, and thus the extent of JT distortion, is directly related to the effective charge doping x_{eff} , the above findings support the assignment of ν_S to a stretch-

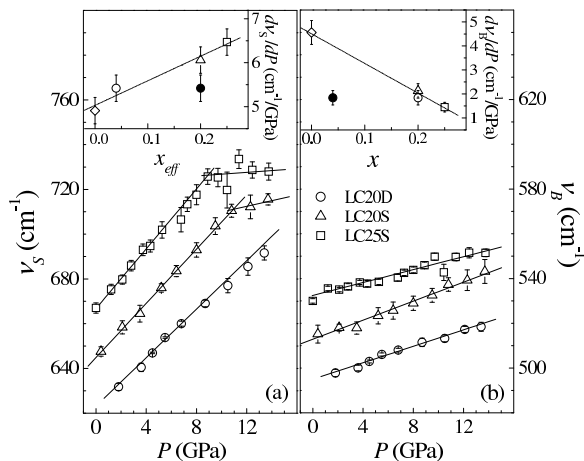


Figure 2: Pressure dependence of phonon frequencies ν_S (a) and ν_B (b) for LC20S, LC20D, and LC25S from Ref. 5. LC20D and LC25S data were up-shifted by 20 cm^{-1} and 40 cm^{-1} respectively. Insets: $d\nu_S/dP$ vs effective doping, x_{eff} (panel a); $d\nu_B/dP$ vs Ca-doping, x (panel b). Data for LaMnO₃ ($x_{eff} = x = 0$) are from Ref. 28. Pressure derivatives for LC20D are also reported as a function of x in panel a) and x_{eff} in panel b) (filled symbols). Solid/dashed lines are guides to the eye.

ing mode strongly sensitive to the JT distortion. Moreover, since the hardening of ν_S indicates local octahedra symmetrization,⁵ the $d\nu_S/dP$ behavior as a function of x_{eff} indicates that, in the LP regime, pressure is more effective in reducing the JT distortion at high x_{eff} , due to the larger number of undistorted Mn⁺⁴ centered octahedra which make the lattice somehow *softer*. On the other hand, the pressure-induced hardening of ν_B is consistent with the assignment of the bending mode. On increasing x the average ionic radius on the rare-earth site is reduced, (La³⁺ is larger than Ca²⁺, Ref. 23) and the available space for bending the apical oxygen ions increases. Therefore at large x , ν_B is less affected by the pressure-induced lattice compression.

In the HP regime $d\nu_B/dP$ remains actually constant for all the samples, whereas $d\nu_S/dP$ almost vanishes above 7 GPa and 9 GPa for LC25S and LC20S respectively. No saturation effects were observed for LC20D over the explored pressure range. The difference between the LP and HP regimes is ascribed to the onset of a new localizing mechanism competing with the pressure induced symmetrization of the MnO₆ octahedron.^{5,6} Since the threshold pressure for the activation of the localizing mechanism appears to decrease on increasing x_{eff} , that is on increasing the metallic character of the system, this finding suggests that the new pressure activated interaction could be somehow related to the effective Mn-Mn hopping integral, rather than to steric effects. These results are in agreement with far infrared measurements⁸ on the same three samples showing that, in samples with metallic ground state, the pressure-induced charge-delocalization process is much more pronounced in LC20S, which exhibits a smaller $T_C = T_{IM}$ and a larger gap at $P = 0$, while at HP both LC20S and LC25S seem to approach the same regime.

The onset of the localizing mechanism can be seen also in the pressure dependencies of the linewidths of the bending (Γ_B) and stretching (Γ_S) phonons of LC20S and LC20D shown in Fig. 3 (a) and (b), respectively, and compared with corresponding results on LC25S from Ref. 5. LC25S shows the largest Γ_S and LC20D the smallest, whereas Γ_B is almost identical in all the three samples. This effect can be interpreted in terms of the disorder of the JT distortion induced by hole doping and it is more evident in LC25S where x and x_{eff} are larger. The absence of any appreciable difference in Γ_B for the three doped samples shows that the bending phonon is not correlated to carrier density and thus to the JT distortion.

A two-regime behavior can be envisaged for Γ_S : on increasing pressure, at first the linewidth remains constant and, above a threshold, it starts to increase linearly. A threshold value of ~ 8 GPa is rather apparent for LC20D whereas it can be roughly evaluated at around 5 GPa for LC20S. In the case of LC25S we can say that the threshold goes to zero and the linewidth linearly increases starting from ambient pressure. The onset of the lineshape broadening could be a precursor of the saturation regime

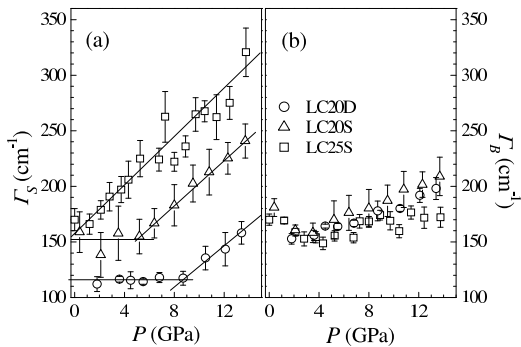


Figure 3: Pressure dependence of the linewidth Γ_S (a) and Γ_B (b) of the stretching and the bending modes respectively, for LC20S and LC20D, compared with results on LC25S from Ref. 5. Solid lines are guides to the eye.

shown by the pressure dependence of ν_S . On the other hand, the linewidth behavior is also consistent with the onset of a pressure-activated localizing interaction, which competes with the *natural* pressure-induced reduction of the JT distortion. Indeed, the competition favors the coexistence of both distorted and undistorted octahedra leading to a remarkable disorder-induced broadening of the JT phonon. With this respect we would like to recall that Raman measurements on LaMnO_3 ($x = x_{eff} = 0$,

shows the onset of a regime characterized by the appearance of domains of less JT distorted octahedra at ~ 8 GPa²⁸ that is at a pressure very close to the threshold found for LC20D ($x_{eff} = 0.04$).

In summary, we reported on high-pressure Raman measurements on $\text{La}_{0.80}\text{Ca}_{0.20}\text{MnO}_{3-\delta}$ with $\delta = 0.00$ and 0.08 . A careful analysis of the phonon pressure dependence as a function of Ca and effective charge doping provided further support to the assignment of the bending and the JT-active stretching octahedral modes. Moreover our results give spectroscopic evidence of the onset of a localizing mechanism at high pressure in metallic ground state manganites, confirming and extending previous data on $\text{La}_{0.75}\text{Ca}_{0.25}\text{MnO}_3$.⁵ The comparison of the present results with literature data allows us to evidence that the greater the metallic degree of the system, the smaller the pressure at which the localizing interaction effect sets in, demonstrating that the strength of the new localizing interaction depends on the effective Mn-Mn hopping integral, which increases on increasing x_{eff} , as well as on increasing pressure. This results in agreement with the theoretical scenario proposed in Ref. 14, in which the localizing super-exchange antiferromagnetic coupling becomes competitive with double exchange at high pressure.

- ¹ A.J. Millis, *Nature* **392**, 147 (1998).
- ² E. Dagotto, *Nanoscale Phase Separation and Colossal Magnetoresistance* (Springer-Verlag, Berlin, 2002).
- ³ C. Zener, *Phys. Rev.* **82**, 403 (1951).
- ⁴ A.J. Millis, P.B. Littlewood, B.I. Shraiman, *Phys. Rev. Lett.* **74**, 5144 (1995).
- ⁵ A. Congeduti, P. Postorino, E. Caramagno, M. Nardone, A. Kumar, and D.D. Sarma, *Phys. Rev. Lett.* **86**, 1251 (2001).
- ⁶ C. Meneghini, D. Levy, S. Mobilio, M. Ortolani, M. Nuñez-Reguero, A. Kumar, and D.D. Sarma, *Phys. Rev. B* **65**, 012111 (2002).
- ⁷ P. Postorino, A. Congeduti, P. Dore, A. Sacchetti, F.A. Gorelli, L. Ulivi, A. Kumar, and D.D. Sarma, *Phys. Rev. Lett.* **91**, 175501 (2003).
- ⁸ A. Sacchetti, M. Cestelli Guidi, E. Arcangeletti, A. Nucara, P. Calvani, M. Piccinini, A. Marcelli, Postorino, *Phys. Rev. Lett.* **96**, 35503 (2006).
- ⁹ C. Cui, T.A. Tyson, Z. Zhong, J.P. Carlo, and Y. Qin, *Phys. Rev. B* **67**, 104107 (2003).
- ¹⁰ C. Cui and T.A. Tyson, *Appl. Phys. Lett.* **83**, 2856 (2003).
- ¹¹ C. Cui, T.A. Tyson, Z. Chen, and Z. Zhong, *Phys. Rev. B* **68**, 214417 (2003).
- ¹² C. Cui and T.A. Tyson, *Appl. Phys. Lett.* **84**, 2856 (2004).
- ¹³ C. Cui and T.A. Tyson, *Phys. Rev. B* **70**, 094409 (2004).
- ¹⁴ A. Sacchetti, P. Postorino, and M. Capone, *N. J. Phys.* **8**, 3 (2006).
- ¹⁵ P.G. Radaelli, G. Iannone, M. Marezio, H.Y. Hwang, S.W. Cheong, J.D. Jorgensen, and D.N. Argyriou, *Phys. Rev. B* **56**, 8265 (1997).
- ¹⁶ Y. Moritomo, H. Kuwahara, and Y. Tokura, *J. Phys. Soc. Jpn.* **66**, 556 (1997).
- ¹⁷ H.Y. Hwang, T.T.M. Palstra, S.-W. Cheong, and B. Batlogg, *Phys. Rev. B* **52**, 15046 (1995).
- ¹⁸ J.J. Nuemeier, M.F. Hundley, J.D. Thompson, and R.H. Heffner, *Phys. Rev. B* **52**, 7006 (1995).
- ¹⁹ K. Kamenev, G. Balakrishnan, M.R. Lees, D.McK. Paul, Z. Arnold, and O. Mikulina, *Phys. Rev. B* **56**, 2285 (1997).
- ²⁰ Y.S. Wang, A.K. Heilman, B. Lorenz, Y.Y. Xue, C.W. Chu, J.P. Franck, and W.M. Chen, *Phys. Rev. B* **60**, R14998 (1999).
- ²¹ B. Lorenz, A.K. Heilman, Y.S. Wang, Y.Y. Xue, C.W. Chu, G.Zhang, and J.P. Franck, *Phys. Rev. B* **63**, 144405 (2001).
- ²² D. P. Kozlenko, S. E. Kichanov, V. I. Voronin, B. N. Savenko, V. P. Glazkov, E. A. Kiseleva and N. V. Proskurnina, *JETP Lett.* **82**, 447 (2005).
- ²³ R.D. Shannon, *Acta Crystallogr. A* **32**, 751 (1976).
- ²⁴ I.O. Troyanchuk, S.V. Trukhanov, H. Szymczak, J. Przewoznik, and K. Bärner, *J. Exp. Theor. Phys.* **93**, 161 (2001).
- ²⁵ T.L. Aselage, D. Emin, S.S. McCreedy, E.L. Venturini, M.A. Rodriguez, J.A. Voigt, and T.J. Headley, *Phys. Rev. B* **68**, 134448 (2003).
- ²⁶ M.N. Iliev, M.V. Abrashev, H.G. Lee, V.N. Popov, Y.Y. Sun, C. Thomsen, R.L. Meng, and C.W. Chu, *Phys. Rev. B* **57**, 2872 (1998).
- ²⁷ M. N. Iliev and M.V. Abrashev, *J. Raman Spectrosc.* **32**, 805 (2001).
- ²⁸ I. Loa, P. Adler, A. Grzechnik, K. Syassen, U. Schwarz, M. Hanfland, G.Kh. Rozenberg, P. Gorodetsky, and M. P. Pasternak, *Phys. Rev. Lett.* **87**, 125501 (2001).